Heterogeneous & Homogeneous & Bio- & Nano-

CHEM**CAT**CHEM

CATALYSIS

Accepted Article

Title: Synthesis of CNTs@POP-salen core-shell nanostructures for catalytic epoxides hydration

Authors: He Li, Mingmei Zhong, Chunzhi Li, Yiqi Ren, Jian Chen, and Qihua Yang

This manuscript has been accepted after peer review and appears as an Accepted Article online prior to editing, proofing, and formal publication of the final Version of Record (VoR). This work is currently citable by using the Digital Object Identifier (DOI) given below. The VoR will be published online in Early View as soon as possible and may be different to this Accepted Article as a result of editing. Readers should obtain the VoR from the journal website shown below when it is published to ensure accuracy of information. The authors are responsible for the content of this Accepted Article.

A Journal of

ChemPubSoc
Europe

WILEY-VCH

www.chemcatchem.org

Synthesis of CNTs@POP-salen core-shell nanostructures for catalytic epoxides hydration

He Li,[a] Mingmei Zhong,[a,b] Chunzhi Li,[a,b] Yiqi Ren,[a,b] Jian Chen,[a,b] and Qihua Yang*[a]

Dedication ((optional))

Abstract: Microporous polymers have been considered as promising heterogeneous catalysts for versatile chemical transformations. However, the mass diffusion barriers through the microporous network still remains a big hindrance. Herein, an efficient and versatile strategy for shortening the mass diffusion pathway through microporous polymer was reported by constructing CNTs@POP-salen core-shell nanostructure. CNTs@POP-Co(salen) could efficiently catalyze the epoxide hydration reaction at H_2O/epoxides ratio as low as 2, demonstrating the efficient cooperation of Co(salen) integrated in the polymer network. CNTs@POP-Co(salen) showed much higher activity than bulk polymer in propylene oxide (PO) hydration reaction (TOF: 3150 versus 1470 h^{-1}) due to the shortened diffusion pathway, which was further confirmed by adsorption experiment using phenol as probe molecule. Our primary results demonstrated the advantages of core-shell nanostructures to improve the catalytic activity of microporous polymers by enhancing the mass diffusion during the catalytic process.

Introduction

Direct epoxide (such as ethylene oxide, propylene oxide) hydration is a very important route for the production of glycols in industry.[1] However, this process is an energy extensive process because non-catalytic hydration process needs a large amount of water for obtaining high glycol selectivity. Though the catalytic hydration of epoxides has aroused extensive research attention, it still lacks of efficient solid catalysts being able to catalyze the hydration reaction with high glycol selectivity at H_2O/epoxide ratio less than 5.[2-7] Previous studies showed that the silica-based nanoreactor with encapsulated Co(Salen) could catalyze the hydration of epoxides at H_2O/epoxide ratio around 2 to afford much higher activity and high selectivity than homogeneous counterpart.[8-9] DFT studies suggested that Co(Salen) goes through bi-molecular activation pathway for the hydration of epoxides.[10-11] The high efficiency of encapsulated Co(salen) in silica-based nanoreactor is mainly attributed to the

enhanced cooperation effect.[8]

Compared with silica-based nanoreactor, porous organic polymers (POPs) are more robust in the presence of water.[12-13] Recently, the POPs with Co(salen) as integrate part of the network have been synthesized and used for the hydration of epoxides at low H_2O/epoxide ratio.[14-15] Due to the cooperative activation nature of Co(salen) for epoxide hydration, the efficient POPs should possess flexible network to enhance the cooperation of two Co(Salen) based on previous reports.[14] The large pore diameter benefits the mass transport during the catalytic process. Though great efforts have been devoted for the synthesis of POPs,[16-18] it still remains a challenge for the synthesis of POPs to fulfill the above requirements.

Shortening the diffusion pathway provides an alternative strategy to improve diffusion rates of guest molecules through porous materials. For example, zeolites nanoparticles, hollow nanosphere, nanosheets, nanoflakes etc. with shortened diffusion pathway exhibit much higher catalytic activity and stability than conventional zeolites in catalytic reactions due to the increased diffusion rates.[19-24] But the methods for tuning the particle size and morphology of POPs are still limited.[25-28] In addition to downsizing the particle size, hybridization of polymer with other solid supports has been used to facilitate the diffusion rates. The sulfonated polystyrene resins physically or chemically hybridized with porous silicas, mesoporous materials, and porous carbons have been reported and the hybridized materials exhibit improved catalytic performance due to increased diffusion rates and exposure degree of active sites.[29-31] The hybrid material with metalloporphyrin-based polymer buried within the macropore of melamine foam could efficiently catalyze the acyl transfer reaction while the polymer itself only afforded low activity.[32]

Carbon nanotubes (CNTs) with tubular morphology, high tensile moduli and strengths have already demonstrated their potential applications as support materials for various transformations.[33-39] Recently, it was demonstrated that a layer of polymers could be formed on the outer surface of CNTs if the monomers could have some interactions with CNTs.[40] This provides an efficient method for tuning the thickness of POPs, and consequently to modulate their catalytic performance. Herein, we reported the synthesis of CNTs@POP-Co(salen) core-shell nanostructures for the hydration of epoxides. Due to the carboxylate-ammonium charge-assisted H-bonds between ethylene diamine and –COOH groups on functionalized CNTs, the core-shell nanostructures with well-defined shell thickness were obtained. CNTs@POP-Co(salen) with flexible polymer on the out surface exhibited much higher activity (TOF: 3150 versus 1470 h^{-1}) than bulk POP-Co(salen) in the hydration of propylene oxide.

[a]   Dr. H. Li, M. Zhong, C. Li, Y. Ren, J. Chen, Prof. Q. Yang
    State Key Laboratory of Catalysis
   *i*ChEM
    Dalian Institute of Chemical Physics
    Chinese Academy of Science
    Dalian 116023, China
    E-mail: yangqh@dicp.ac.cn
[b]   M. Zhong, C. Li, Y. Ren, J. Chen
    University of Chinese Academy of Sciences
    Beijing 100049, China

    Supporting information for this article is given via a link at the end of the document.((Please delete this text if not appropriate))

Results and Discussion

CNTs@POP-salen was synthesized using ethylene diamine and 1,3,5-tris(3'-tert-butyl-4'-hydroxy-5'-formylphenyl)benzene (TBHFPB) as monomers and nitric acid treated CNTs (the CNTs ultilized in the text unless otherwise stated) as support materials. After nitric acid treatment, the functionalized CNTs still possessed tubular morphology with outer and inner diameter of 15~45 and 4~9 nm, respectively (Figure 1A). The direct mixing of the monomers and non-functionalized CNTs resulted in the formation of composite materials with phase separated POPs and CNTs (denoted as CNTs-POP-salen) on the basis of TEM characterization (Figure 1B). Alkordi and co-workers reported the one-pot synthesis of POP@G composite using different POPs and graphene.[41-43] The phase separated POPs and CNTs was possibly caused by the fast precipitation of POP-salen in our case. In order to obtain the core-shell composite material, a two-step procedure was employed. Considering that nitric acid treated CNTs have -COOH functional group (the stretching vibration of characteristic -COOH at 1700 cm^{-1} was clearly observed in the FT-IR spectrum shown in Figure 2A), ethylene diamine was firstly adsorbed on the surface of the functionalized CNTs.[44] The FT-IR spectrum of ethylene diamine treated CNTs clearly showed the characteristic peaks of -NH- and -CH$_2$- at 1590 and 1470 cm^{-1}, indicating that ethylene diamine could be adsorbed on nitric acid treated CNTs via carboxylate-ammonium charge-assisted H-bonds.[45-47] The subsequent addition of TBHFPB resulted in the successful formation of CNTs@POP-salen-n (n refers to mass ratio of TBHFPB to CNTs) core-shell nanostructure.
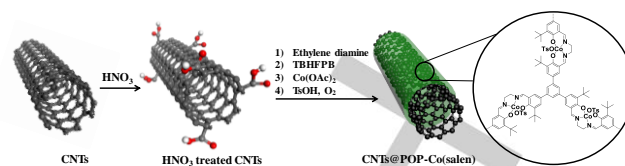
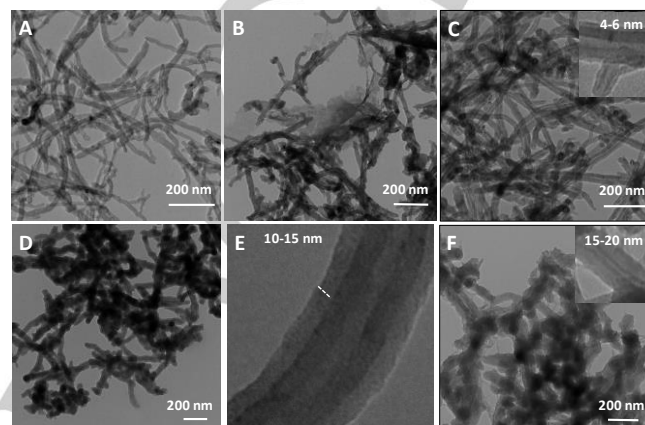**Scheme 1.** Schematic illustration for the synthesis of CNTs@POP-Co(salen).

Figure 1. TEM images of (A) nitric acid treated CNTs, (B) CNTs-POP-salen, (C) CNTs@POP-salen-0.5, (D, E) CNTs@POP-salen-1 and (F) CNTs@POP-salen-2.
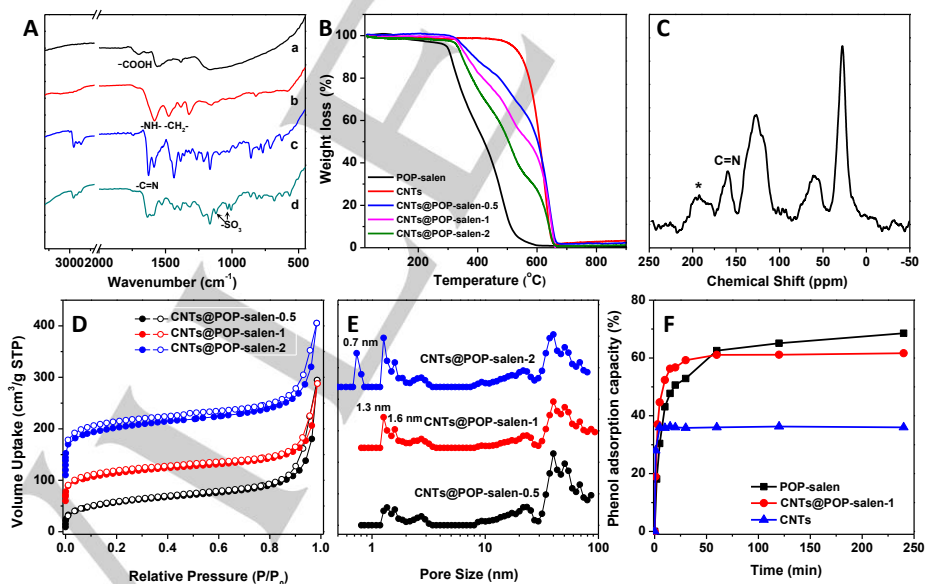

Figure 2. (A) FT-IR spectra of (a) CNTs after nitric acid treatment, (b) nitric acid treated CNTs after adsorbed with ethylene diamine, (c) CNTs@POP-salen-1 and (d) CNTs@POP-Co(salen)-1, (B) TG curves of CNTs, POP-salen and CNTs@POP-salen-n, (C) ^{13}C CP-MAS NMR spectrum of CNTs@POP-salen-1 (star refers to sideband), (D) N$_2$ sorption isotherms and (E) NLDFT pore-size distribution curves of CNTs@POP-salen-n, (F) the phenol adsorption curves of CNTs@POP-salen-1, POP-salen and CNTs in water.

The TEM and SEM images clearly showed that all CNTs@POP-salen-n samples had nanotube morphology similar to pristine CNTs, indicating the formation of POP-salen around functionalized CNTs (Figure 1C-F and S1). A uniformly coated polymer layer around CNTs could be clearly identified from the obvious contrast difference between POP-salen and CNTs in the TEM image, which confirmed the formation of core-shell nanostructures with CNTs as core and POP-salen as shell. Via varying the amounts of monomer in the initial mixture, the average shell thickness could be precisely adjusted from 4~6 nm to 15~20 nm. On the basis of thermal gravimetric analysis (Figure 2B), the decomposition temperature of POP-salen and CNTs@POP-salen started at 290 °C and 320 °C, respectively. The increase in decomposition temperature for the composite materials indicated the existence of interactions (e.g. carboxylate-ammonium charge-assisted H-bonds, π-π interactions) between the polymer and CNTs. CNTs@POP-salen-0.5, CNTs@POP-salen-1 and CNTs@POP-salen-2 have N content respectively of 1.7, 2.5 and 3.2 mmol/g, corresponding to polymer contents of 34 wt%, 50 wt% and 64 wt% on the basis of C, H, N elemental analysis (Table 1).

Table 1. Chemical and physical parameters of CNTs@POP-salen-n, POP-salen, and CNTs.

Sample	N content (mmol/g)[a]	Polymer thickness (nm)	BET surface area (m²/g)	Pore size (nm)
CNTs	0	0	161	-
CNTs@POP-salen-0.5	1.7	4~6	204	1.3, 1.6
CNTs@POP-salen-1	2.5	10~15	225	1.3, 1.6
CNTs@POP-salen-2	3.2	15~20	353	0.7, 1.3, 1.6
POP-salen[14]	5.0	-	464	0.7, 1.3, 1.6

[a] N content was measured by elemental analysis.

The composition of representative CNTs@POP-salen-1 was characterized by FT-IR spectroscopy. The characteristic stretching vibration of C=N at 1625 cm⁻¹, C-H vibrations in the region of 2850~3000 cm⁻¹, and C-C vibrations of aromatic ring at 1590 and 1436 cm⁻¹ could be clearly observed in the FT-IR spectrum (Figure 2A), suggesting the successful formation of salen skeleton in the composite. ¹³C CP MAS NMR spectrum of CNTs@POP-salen-1 showed characteristic signals at 20~50 ppm assigned to aliphatic carbons of tert-butyl, 60 ppm for -CH₂, 120~145 ppm for the carbons of the aromatic ring, 158 ppm for C-O and 165 ppm for C=N (Figure 2C).[14,48] The combined results of FT-IR and ¹³C CP MAS NMR characterizations confirmed the formation of POP-salen based composite materials.

The porosity of CNTs@POP-salen-n was investigated by N₂ sorption analysis (Figure 2D and Table 1). All CNTs@POP-

salen-n showed typical type I isotherm patterns with a steep increment at low pressure, indicating that all the samples have microporous structure. The significant increase of N₂ uptake at P/P₀ from 0.9 to 1.0 demonstrated the existence of intervoid space, similar to functionalized CNTs (Figure S2). All CNTs@POP-salen materials had higher BET surface area than pristine CNTs, and the BET surface area increased with the increment of polymer content. This is reasonable because the BET surface area of CNTs is smaller than that of POP-salen (Scheme S1). Compared with CNTs, all CNTs@POP-salen materials gave new pore size distributions at 1.3 and 1.6 nm derived from POP-salen (Figure 2E). It should be noted that CNTs@POP-salen-2 gave an additional micropore at 0.7 nm, which was also observed for POP-salen.[14] This suggested that CNTs@POP-salen with polymer thickness > 15 nm had similar porous structure to the pure polymer.
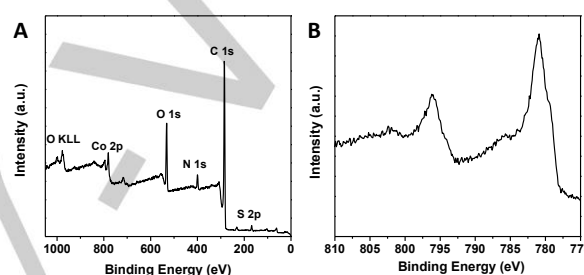
Figure 3. (A) XPS full scan survey and (B) high resolution XPS Co 2p spectrum of CNTs@POP-Co(salen)-1.

CNTs@POP-salen-n samples were converted to CNTs@POP-Co(salen)-n by coordination with cobalt acetate followed by an oxidation process in open air in the presence of *p*-toluenesulfonic acid (TsOH). The cobalt content of CNTs@POP-Co(salen)-0.5, CNTs@POP-Co(salen)-1 and CNTs@POP-Co(salen)-2 are respectively 0.27, 0.41 and 0.51 mmol/g as analyzed by inductively coupled plasma atomic emission spectroscopy (ICP-AES). The composition of CNTs@POP-Co(salen)-n was investigated by FT-IR spectroscopy using CNTs@POP-Co(salen)-1 as representative sample (Figure 2A). Two new peaks at 1120 cm⁻¹ and 1000 cm⁻¹ corresponding to asymmetric stretching vibration and symmetric vibration peak of sulfonyl groups in the FT-IR spectrum of CNTs@POP-Co(salen)-1 confirmed the formation of salen-Co^{III} in the composite. X-ray photoelectron spectroscopy (XPS) survey result of CNTs@POP-Co(salen)-1 clearly showed the feature peaks of C 1s, N 1s, O 1s and KLL, S 2p and Co 2p (Figure 3A). The XPS spectrum of Co 2p core level showed one doublet corresponding to Co 2p$_{3/2}$ and Co 2p$_{1/2}$ spin–orbit split, and the binding energy for Co 2p$_{1/2}$ of CNTs@POP-Co(salen)-1 was 796.2 eV, identical to the reported homogeneous salen-Co^{III} complex (Figure 3B).[14] This indicated that Co(salen) integrated in the composite has similar coordination environment to the homogeneous salen-Co^{III} complex. The TEM and SEM images showed that all CNTs@POP-Co(salen)-n materials had almost identical core-shell nanostructure and shell thickness to corresponding CNTs@POP-salen-n samples (Figure S3). The

BET surface area of CNTs@POP-Co(salen)-n decreased in comparison to CNTs@POP-salen-n, possibly due to the occupation of Co cations in the polymer (Figure S4).[49]

Table 2. Comparison the catalytic performances of CNTs@POP-Co(salen)-n, POP-Co(salen) and CNTs-POP-Co(salen) in PO hydration reaction.[a]

Catalyst	Co content (mmol/g)[b]	TOF (h^{-1})	Yield (%)	Sel. (%)
CNTs	--	--	9	-
CNTs@POP-salen-1	--	--	n.d	-
CNTs@POP-Co(salen)-0.5	0.27	1008	55	99
CNTs@POP-Co(salen)-1	0.41	3150	93	99
CNTs@POP-Co(salen)-2	0.51	2025	84	99
POP-Co(salen)	1.0	1470	83	99
CNTs-POP-Co(salen)	0.75	960	60	99

[a] S/C = 500, H_2O/PO molar ratio = 2, 40 °C, the TOF was calculated with yield < 30%, n.d is not detected, reaction time 2 h, the only detected product is 1,2-propanediol. [b] Co content was measured by ICP analysis.
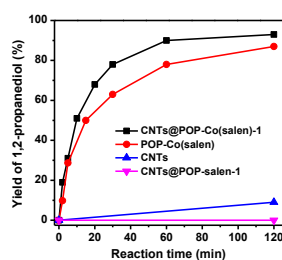

Figure 4. The reaction profiles with time for different types of catalysts in the hydration of PO (S/C = 500, H_2O/PO molar ratio = 2, 40 °C).

The catalytic performance of CNTs@POP-Co(salen)-1 was tested in the hydration of propylene oxide (PO) with H_2O/PO molar ratio of 2 at 40 °C (Table 2 and Figure 4). The control experiments with CNTs as catalyst only afforded 9% yield of 1,2-propanediol and no product was observed with CNTs@POP-salen-1 as catalyst. With CNTs@POP-Co(salen)-1 as catalyst, PO could be smoothly converted to 1,2-propanediol with 93% yield and 99% selectivity to 1,2-propanediol within 2 hours, revealing that salen-Co^{III} is the active site for PO hydration reaction. This indicated that Co(salen) integrated in the polymer network could work via a cooperative pathway based on previous reports.[14] The kinetic plots showed that the reaction rate of CNTs@POP-Co(salen)-1 is much faster than that of POP-Co(salen). The calculated turnover frequency (TOF) for CNTs@POP-Co(salen)-1 is 3150 h^{-1}, more than 2 times that of POP-Co(salen) (1470 h^{-1}). This verifies the efficiency of the core-shell nanostructures in improving the catalytic performance of microporous polymer. POP-Co(salen) and CNTs@POP-

Co(salen)-1 have similar polymer network and BET surface area (100 vs 98 m^2/g) (Figure S4), thus the different catalytic activity may be related with their morphology. POP-Co(salen) has microspherical morphology with particle size of ~1 μm and CNTs@POP-Co(salen)-1 has a core-shell nanostructure with polymer thickness of 10 to 15 nm.[14] In comparison with POP-Co(salen), the diffusion distance of PO and H_2O was much shorter through CNTs@POP-Co(salen)-1 than through POP-Co(salen), which may help to increase the reaction rate. Additionally, the TOF of phase separated CNT-POP-Co(salen) was much lower than that of CNTs@POP-Co(salen)-1 (960 vs 3150 h^{-1}), this further proved the efficiency of CNTs@POP-Co(salen)-1 core-shell nanostructure in catalysis.

The diffusion of guest molecules throughout CNTs@POP-salen-1 was investigated and compared with CNTs and POP-salen using phenol as probe molecules in water (Figure 2F). Both CNTs@POP-salen-1 and POP-salen showed fast phenol adsorption rate in the initial 30 min. After that, the adsorption rate slowed down and reached the adsorption equilibrium. To exclude the influence of CNTs on the adsorption behavior of CNTs@POP-salen-1, the adsorption behavior of CNTs was also tested under similar conditions. Although CNTs showed a fast phenol adsorption rate, the phenol adsorption capacity of CNTs was only 3.46 mg/g. The adsorption capacity of CNTs@POP-salen-1 was 5.98 mg/g, corresponding to 8.50 mg/g polymer. The higher adsorption capacity of CNTs@POP-salen-1 than CNTs showed that polymer mainly contributed to the phenol adsorption. CNTs@POP-salen-1 showed faster adsorption rate than POP-salen, indicating that the diffusion rate of phenol is faster in CNTs@POP-salen-1 than POP-salen. Furthermore, POP-salen gave a less phenol adsorption capacity than CNTs@POP-salen-1 (6.72 versus 8.50 mg/g polymer). This result suggested CNTs@POP-Co(salen)-1 with a shortened diffusion distance could adsorb more guest molecules. Based on the results of phenol adsorption, it could come to a conclusion that the enhanced activity of CNTs@POP-Co(salen)-1 in PO hydration reaction was possibly due to its shortened diffusion pathway.

The shell-thickness of CNTs@POP-Co(salen)-n on the catalytic performances in PO hydration reactions was investigated (Table 2). The TOF of CNTs@POP-Co(salen)-n increased enormously as the thickness of polymer layer increased from 4~6 nm to 10~15 nm (1008 vs 3150 h^{-1}). Further increasing the thickness of polymer layer caused the decrease in activity. Previous studies showed that salen-Co^{III} catalyzes the epoxide hydration reaction via a dual-molecular cooperative activation pathway.[50-52] Thus, a flexible network is necessary for obtaining high activity. The TG analysis suggested the existence of interactions among CNTs and polymers. For CNTs@POP-Co(salen)-0.5, the flexibility of the polymer layer decreased due to their adhering to the CNTs. With polymer thickness increasing, the diffusion resistance increased. Consequently, there was a balance between the polymer flexibility and mass diffusion resistance. As a result, CNTs@POP-Co(salen)-1 with optimized polymer flexibility and mass diffusion resistance afforded the highest activity.

The influence of H_2O/epoxide ratio and S/C ratio on the catalytic performance of composite materials was investigated using CNTs@POP-Co(salen)-1 as model catalyst in PO hydration reaction (Figure 5). With H_2O/PO molar ratio in the range of 1 to 5, CNTs@POP-Co(salen)-1 could smoothly catalyze the hydration reaction to afford the 1,2-propanediol yield ranging from 86% to 99%. As the H_2O/PO molar ratio increased from 1 to 5, the TOF firstly increased and reached a plateau (3225 h⁻¹) at H_2O/PO molar ratio of 4. These results showed that CNTs@POP-Co(salen)-1 could efficiently catalyze epoxide hydration in a wide range of H_2O/epoxide molar ratio.
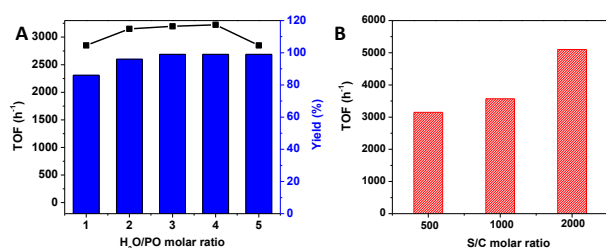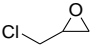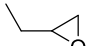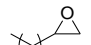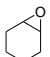

Figure 5. Catalytic performances of CNTs@POP-Co(salen)-1 in PO hydration reaction at different (A) H_2O/PO (reaction time, 3 h) and (B) S/C molar ratios.

Table 3. The catalytic performances of CNTs@POP-Co(salen)-1 for the hydration of various epoxides.[a]

Substrate	Reaction time (h)	Yield of diol (%)	Selectivity (%)
(epoxide)	6	94	94[b]
Cl (epichlorohydrin)	6	99	99
(1,2-butane oxide)	6	96	99
(1,2-epoxyhexane)	4	93	97
(cyclohexene oxide)	48	62	91

[a] S/C = 500, 40 ℃, H_2O/epoxide molar ratio = 2. [b] The reaction was conducted under 1 MPa of N_2, H_2O/ethylene oxide molar ratio = 5, the by-product is diethylene glycol.

The TOF of homogeneous Co(salen) decreased as S/C increased as we previously observed.[14] This is due to the fact that low catalyst concentration does not favour the generation of cooperative activation effect. As for CNTs@POP-Co(salen)-1, the active sites are located in the polymer network, the density of the active sites should remain the same regardless of the variation in S/C ratio. To our delight, the TOF of CNTs@POP-

Co(salen)-1 increased enormously from 3150 to 5100 h⁻¹ as the S/C ratio increased from 500 to 2000 (Figure 5B). This result confirms the existence of enhanced cooperative activation effect for the solid catalysts.

Encouraged by the high activity of CNTs@POP-Co(salen)-1 in PO hydration reaction, the substrate scope was further investigated (Table 3). CNTs@POP-Co(salen)-1 could smoothly catalyze the hydration of ethylene oxide, epichlorohydrin, 1,2-butane oxide, and 1,2-epoxyhexane to afford high conversion and high selectivity. Even the challenging substrate, cyclohexene oxide, could also be converted to the corresponding glycol with 62% yield and 91% selectivity in 48 h. These results confirms that CNTs@POP-Co(salen)-1 has a wide substrate scope.

In order to investigate the stability and the heterogeneous nature of CNTs@POP-Co(salen)-1 in PO hydration reaction, the filtration experiment was performed by removing the catalyst out of the catalytic system at the 1,2-propanediol yield approaching 49%. Almost no further increase in the glycol yield could be found by further stirring the filtrate for another 2 h. This result confirms that the PO hydration was indeed catalyzed by the solid catalyst. Furthermore, the recycle stability of CNTs@POP-Co(salen)-1 was tested in PO hydration and compared with POP-Co(salen) (Figure 6A). The obvious decrease in the activity was observed for POP-Co(salen) during the recycling process. Compared with POP-Co(salen), CNTs@POP-Co(salen)-1 showed much higher recycling stability. Though the recycle stability of POP-Co(salen) could be improved by the formation of hybrid core-shell nanostructure, the decrease in product yield was observed after the fourth cycle. The TEM image of CNTs@POP-Co(salen)-1 after 4 runs clearly showed the core-shell nanostructures, indicating that the deactivation of CNTs@POP-Co(salen)-1 is not due to the change in morphology (Figure 6B). During the regeneration process of CNTs@POP-Co(salen)-1 in acid medium, the leaching of Co cations was observed. This suggests the deactivation of CNTs@POP-Co(salen)-1 is possibly due to the breakage of C=N bond in salen unit. To further improve the stability of CNTs@POP-Co(salen)-1 is under investigation in our group.
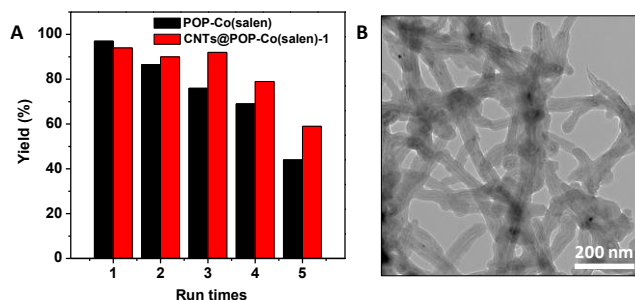

Figure 6. (A) Recycling stability of CNTs@POP-Co(salen)-1 and POP-Co(salen) in the hydration of PO (S/C = 500, 40 °C, H_2O/PO molar ratio = 2, t = 3 h), (B) TEM image of CNTs@POP-Co(salen)-1 after the fourth catalytic cycle.

Conclusions

In summary, CNTs supported POP-salen with uniform core-shell nanostructures were facilely prepared. The thickness of the polymer layer could be facilely adjusted by controlling the amount of the monomer in the initial synthesis. The TOF of CNTs@POP-Co(salen)-1 was more than 2 times that of POP-Co(salen) in PO hydration reaction. This verifies the efficiency of the core-shell nanostructures in improving the catalytic activity of microporous polymer by shortening the diffusion pathway as demonstrated by phenol adsorption experiment. There was a balance between the polymer flexibility and mass diffusion resistance. As a result, CNTs@POP-Co(salen)-1 with optimized polymer flexibility and mass diffusion resistance afforded the highest activity. Moreover, CNTs@POP-Co(salen)-1 showed much higher recycling stability than bulk polymer in epoxide hydration reactions. The formation of core-shell nanostructures is an efficient strategy for improving the mass diffusion rate through the microporous networks.

Experimental Section

Chemicals and reagents

All chemicals were used as received unless otherwise stated. Carbon nanotubes with a length of 0.5~2 μm and an OD (outer diameter) of 20~50 nm were purchased from Timesnano (Chengdu Organic Chemicals Co. Ltd, China). 1,3,5-Tris(3'-tert-butyl-4'-hydroxy-5'-formylphenyl)benzene (TBHFPB),[53] POP-Co(salen) were synthesized according to the literature method.[14]

Characterization

Transmission electron microscopy (TEM) characterization was performed by using a HITACHI HT7700 microscope at an acceleration voltage of 100 kV. Before measurement, the samples were fully dispersed in ethanol and then deposited on a holey carbon film on a Cu grid. Scanning electron microscopy (SEM) was undertaken on a FEI Quanta 200F scanning electron microscope operating at an acceleration voltage of 20-30 kV. Thermogravimetric analysis (TGA) was performed under an air atmosphere with a heating rate of 10 °C/min by using a NETZSCH STA-449F3 thermogravimetric analyzer. FT-IR spectra were collected using a Nicolet Nexus 470 IR spectrometer (with KBr pellets) in the range of 400-4000 cm^{-1}. Solid state NMR experiments were carried out on a VARIAN Infinity plus spectrometer equipped with a 2.5 mm probe. The ^{13}C CP MAS spectra were recorded using a delay of 3.0 s and a magic angle spinning rate of 8 kHz. The nitrogen physical adsorption measurement was carried out on a Micromeritics ASAP 2020 volumetric adsorption analyzer. Before the measurements, the samples were carefully degassed at 393 K for 6 h. The BET surface area was evaluated from the data in the relative pressure range P/P_0 from 0.05 to 0.25. The pore diameter was determined from the adsorption branch by nonlocal density functional theory (NLDFT) method. X-ray photoelectron spectroscopy (XPS) was recorded on a Thermofisher ESCALAB 250Xi apparatus by using AlKα (h_λ = 1486.6 eV) as the excitation light source. C, H, N elemental analysis was performed with an Oxygen/Nitrogen/Hydrogen Analyzer (EMGA-930, HORIBA, Japan) and a Carbon/Sulfur Analyzer (EMIA-8100, HORIBA, Japan). Cobalt content of the composites was determined by PLASAM-SPEC-II inductively coupled plasma atomic emission spectrometry (ICP) by digesting the sample in HNO_3/H_2SO_4 (1:1, v/v).

Synthesis

Syntheis of CNTs@POP-salen-n: Raw CNTs were treated in aqueous HNO_3 solution following a procedure adapted from the literature. Briefly, 3 g of CNTs were suspended in 150 mL of concentrated HNO_3 (68 wt%) and refluxed at 120 °C for 10 h. After cooling down to room temperature, the solid product was filtered, washed with deionized water until the pH value of the filtrate was around 7. The product was dried at 100 °C for 12 h.

120 mg of HNO_3 treated CNTs was dispersed in 20 mL ethanol. After ultrasonic treatment for 30 min, 20 μL (0.3 mmol) of ethanediamine was added. The mixture was stirred for another 10 min, followed by the slowly addition of 120 mg (0.2 mmol) of TBHFPB which was dissolved in 2 mL of dichloromethane. After stirring for 30 min at room temperature, the mixture was refluxed for 3 h at 80 °C. After cooling down to room temperature, the solid product was filtered, washed with ethanol and dried under vacuum at room temperature for 12 h. The product was denoted as CNTs@POP-salen-1.

CNTs@POP-salen-0.5 and CNTs@POP-salen-2 was synthesized under a similar procedure as described above, with the differences in the loading amount of ethanediamine and TBHFPB.

Synthesis of CNTs@POP-Co(salen)-n: CNTs@POP-Co(salen)-n was prepared via a two-step procedure. At first, Co(OAc)$_2$·4H$_2$O (37.4 mg, 0.15 mmol) was dissolved in a mixture of H$_2$O (0.1 mL) and ethanol (2.5 mL). The mixture was slowly added to a solution of CNTs@POP-salen-1 (60 mg) dispersed in toluene (2.5 mL), the reaction mixture was heated to reflux at 100 °C for 2 h under nitrogen. After cooling down to room temperature, the solid was collected by filtration, washed with methanol, ethanol and water, after that, the obtained solid was dried under vacuum at room temperature for 12 h. The product was denoted as CNTs@POP-Co^{II}(salen)-1.

140 mg of CNTs@POP-Co^{II}(salen)-1 was dispersed in 5 mL ethanol, then a solution of TsOH (50 mg, 0.26 mmol) dissolved in 10 mL EtOH was added dropwise and the mixture was further stirred under air atmosphere at room temperature for 3 h. The solid was collected by filtration, washed with ethanol and dried under vacuum at room temperature for 12 h. The product was denoted as CNTs@POP-Co(salen)-1.

CNTs@POP-Co(salen)-0.5 and CNTs@POP-Co(salen)-2 were synthesized under similar procedures as described above, with the exception of the loading amount of cobalt acetate and TsOH.

General procedures for the adsorption of phenol

An aqueous solution of phenol with a concentration of 0.5 mmol/L was prepared for the adsorption test. 50 mg CNTs, POP-salen or CNTs@POP-salen-1 was added into a 50 mL round flask which contains 10 mL of the prepared phenol solution, then it was stirred at 500 rpm under room temperature. After a certain time, a small amount of the solution was taken out. The concentration of the solution was detected using UV-vis spectroscopy. The adsorption capacity was obtained after 120 min.

General procedures for the epoxide hydration reaction

A desired amount of solid catalyst, PO, and a given number of H$_2$O was added in a 10 mL Schlenk tube, and then the reaction mixture was stirred at 40 °C for 3 h. After cooling to room temperature, octanol (as the internal standard, 48 μL, 40 mg) was added to the mixture and the solid

FULL PAPER

WILEY-VCH

catalyst was separated by filtration. The liquid phase was diluted with ethanol and then analysed by gas chromatography (GC) using a PEG column (30 m × 0.25 mm × 0.25 mm).

For ethylene oxide hydration reaction, a procedure similar to that outlined above was utilized with the exception that the reaction was conducted in a 15 mL autoclave and charged with 1 MPa of nitrogen, the water/ethylene oxide molar ratio is 5.

For other substrates, a procedure similar to the hydration of PO with the exception that epichlorohydrin, 1,2-epoxybutane, 1,2-epoxyhexane or cyclohexane oxide was used instead of propylene oxide.

For the catalyst recycling, the solid catalyst filtered from the reaction mixture was regenerated by dispersing in EtOH containing TsOH (1~1.5 eq.) under air for 3 h. After washing with EtOH and dried under vacuum, the regenerated solid catalyst was used in the next cycle.

Acknowledgements

[1]   H. Yue, Y. Zhao, X. Ma, J. Gong, *Chem. Soc. Rev.* **2012**, *41*, 4218-4244.

[2]   B. Tang, W. Dai, G. Wu, N. Guan, L. Li, M. Hunger, *ACS Catal.* **2014**, *4*, 2801-2810.

[3]   W. Dai, C. Wang, B. Tang, G. Wu, N. Guan, Z. Xie, M. Hunger, L. Li, *ACS Catal.* **2016**, *6*, 2955-2964.

[4]   A. Modak, P. Bhanja, A. Bhaumik, *Chem. Eur. J.* **2018**, *24*, 14189-14197.

[5]   X. Lu, H. Xu, J. Yan, W. Zhou, A. Liebens, P. Wu, *J. Catal.* **2018**, *358*, 89-99.

[6]   S. S. Poly, S.M.A. H. Siddiki, A. S. Touchy, S. Yasumura, T. Toyao, Z. Maeno, K. Shimizu, *J. Catal.* **2018**, *368*, 145-154.

[7]   Y. Li, F. Yu, W. He, W. Yang, *RSC Adv.* **2015**, *5*, 2550-2561.

[8]   B. Li, S. Bai, X. Wang, M. Zhong, Q. Yang, C. Li, *Angew. Chem.* **2012**, *124*, 11685-11689; *Angew. Chem. Int. Ed.* **2012**, *51*, 11517-11521.

[9]   M. Zhong, Y. Zhao, Q. Yang, C. Li, *J. Catal.* **2016**, *338*, 184-191.

[10]   K. Venkatasubbaiah, C. S. Gill, T. Takatani, C. D. Sherrill, C. W. Jones, *Chem. Eur. J.* **2009**, *15*, 3951-3955.

[11]   K. Sun, W. Li. Z. Feng, C. Li, *Chem. Phys. Lett.* **2009**, *470*, 259-263.

[12]   S. Kandambeth, A. Mallick, B. Lukose, M. V. Mane, T. Heine, R. Banerjee, *J. Am. Chem. Soc.* **2012**, *134*, 19524-19527.

[13]   R. Dawson, A. I. Cooper, D. J. Adams, *Prog. Polym. Sci.* **2012**, *37*, 530-563.

[14]   M. Zhong, H. Li, J. Chen, L. Tao, C. Li, Q. Yang, *Chem. Eur. J.* **2017**, *23*, 11504-11508.

[15]   Z. Dai, Q. Sun, F. Chen, S. Pan, L. Wang, X. Meng, J. Li, F.-S. Xiao, *ChemCatChem* **2016**, *8*, 812-817.

[16]   X. Zou, H. Ren, G. Zhu, *Chem. Commun.* **2013**, *49*, 3925-3936.

[17]   Y. Zhang, S. N. Riduan, *Chem. Soc. Rev.* **2012**, *41*, 2083-2094.

[18]   Y. Xu, S. Jin, H. Xu, A. Nagai, D. Jiang, *Chem. Soc. Rev.* **2013**, *42*, 8012-8031.

[19]   G. Prieto, H. Tüysüz, N. Duyckaerts, J. Knossalla, G. Wang, F. Schüth, *Chem. Rev.* **2016**, *116*, 14056-14119.

[20]   Y. Li, L. Li, J. Yu, *Chem* **2017**, *3*, 928-949.

[21]   Y. Liu, X. Zhou, X. Pang, Y. Jin, X. Meng, X. Zheng, X. Gao, F.-S. Xiao, *ChemCatChem* **2013**, *5*, 1517-1523.

[22]   Y. Jin, X. Chen, Q. Sun, N. Sheng, Y. Liu, C. Bian, F. Chen, X. Meng, F.-S. Xiao, *Chem. Eur. J.* **2014**, *20*, 17616-17623.

[23]   S. Li, C. Aquino, L. Gueudré, A. Tuel, Y. Schuurman, D. Farrusseng, *ACS Catal.* **2014**, *4*, 4299-4303.

[24]   W. Ren, Z. Hua, T. Ge, X. Zhou, L. Chen, Y. Zhu, J. Shi, *Chin. J. Catal.* **2015**, *36*, 906-912.

[25]   G. Das, T. Skorjanc, S. K. Sharma, T. Prakasam, C. Platas-Iglesias, D. S. Han, J. Raya, J.-C. Olsen, R. Jagannathan, A. Trabolsi, *ChemNanoMat* **2018**, *4*, 61-65.

[26]   H. Bunzen, M. Grzywa, M. Hambach, S. Spirkl, D. Volkmer, *Cryst. Growth Des.* **2016**, *16*, 3190-3197.

[27]   C. Wan, X. Huang, *Mater. Today Commun.* **2017**, *11*, 38-60.

[28]   Q. Li, S. Razzaque, S. Jin, B. Tan, *Sci. China Chem.* **2017**, *60*, 1056-1066.

[29]   X. Zhang, L. Zhang, Q. Yang, *J. Mater. Chem. A* **2014**, *2*, 7546-7554.

[30]   X. Zhang, Y. Zhao, S. Xu, Y. Yang, J. Liu, Y. Wei, Q. Yang, *Nat. Commun.* **2014**, *5*, 3170.

[31]   R. Zhong, B. F. Sels, *Appl. Catal. B* **2018**, *236*, 518-545.

[32]   K. Wu, J. Guo, C. Wang, *Angew. Chem.* **2016**, *128*, 6117-6121; *Angew. Chem. Int. Ed.* **2016**, *55*, 6013-6017.

[33]   Z. Spitalsky, D. Tasis, K. Papagelis, C. Galiotis, *Prog. Polym. Sci.* **2010**, *35*, 357-401.

[34]   J. M. Planeix, N. Coustel, B. Coq, V. Brotons, P. S. Kumbhar, R. Dutartre, P. Geneste, P. Bernier, P. M. Ajayan, *J. Am. Chem. Soc.* **1994**, *116*, 7935-7936.

[35]   M. Gholinejad, Z. Naghshbandi, C. Nájera, *ChemCatChem* **2019**, DOI: 10.1002/cctc.201802101.

[36]   T. Kitanosono, P. Xu, S. Kobayashi, *Science* **2018**, *362*, 311-315.

[37]   Z. Chen, Z. Guan, M. Li, Q. Yang, C. Li, *Angew. Chem.* **2011**, *123*, 5015-5019; *Angew. Chem. Int. Ed.* **2011**, *50*, 4913-4917.

[38]   F. Xu, S. Jin, H. Zhong, D. Wu, X. Yang, X. Chen, H. Wei, R. Fu, D. Jiang, *Sci. Rep.* **2015**, *5*, 8225.

[39]   R. R. Haikal, A. B. Soliman, M. Amin, S. G. Karakalos, Y. S. Hassan, A. M. Elmansi, I. H. Hafez, M. R. Berber, A. Hassanien, M. H. Alkordi, *Appl. Catal. B* **2017**, *207*, 347-357.

[40]   S. Jayakumar, H. Li, J. Chen, Q. Yang, *ACS Appl. Mater. Interfaces* **2018**, *10*, 2546-2555.

[41]   A. B. Soliman, R. R. Haikal, Y. S. Hassan, M. H. Alkordi, *Chem. Commun.* **2016**, *52*, 12032-12035.

[42]   A. B. Soliman, M. H. Hassan, T. N. Huan, A. A. Abugable, W. A. Elmehalmey, S. G. Karakalos, M. Tsotsalas, M. Heinle, M. Elbahri, M. Fontecave, M. H. Alkordi, *ACS Catal.* **2017**, *7*, 7487-7854.

[43]   A. B. Soliman, M. H. Hassan, A. A. Abugable, S. G. Karakalos, M. H. Alkordi, *ChemCatChem* **2017**, *9*, 2946-2951.

[44]   Y. C. Jung, N. G. Sahoo, J. W. Cho, *Macromol. Rapid Commun.* **2006**, *27*, 126-131.

[45]   M. D. Ward, *Chem. Commun.* **2005**, 5838-5842.

[46]   S. Chand, S. C. Pal, A. Pal, Y. Ye, Q. Lin, Z. Zhang, S. Xiang, M. C. Das, *Chem. Eur. J.* **2019**, *25*, 1691-1695.

[47]   G. Xing, T. Yan, S. Das, T. Ben, S. Qiu, *Angew. Chem.* **2018**, *130*, 5443-5447; *Angew. Chem. Int. Ed.* **2018**, *57*, 5345-5349.

[48]   Y. Xie, T. Wang, X. Liu, K. Zou, W. Deng, *Nat. Commun.* **2013**, *4*, 1960.

[49]   H. Li, X. Feng, P. Shao, J. Chen, C. Li, S. Jayakumar, Q. Yang, *J. Mater. Chem. A* **2019**, *7*, 5482-5492.

[50]   L. P. C. Nielsen, S. J. Zuend, D. D. Ford, E. N. Jacobsen, *J. Org. Chem.* **2012**, *77*, 2486-2495.

[51]   W. Ren, Y. Wang, R. Zhang, J. Jiang, X. Lu, *J. Org. Chem.* **2013**, *78*, 4801-4810.

[52]   L. P. C. Nielsen, C. P. Stevenson, D. G. Blackmond, E. N. Jacobsen, *J. Am. Chem. Soc.* **2004**, *126*, 1360-1362.

[53]   H. Li, B. Xu, J. He, X. Liu, W. Gao, Y. Mu, *Chem. Commun.* **2015**, *51*, 16703-16706.

WILEY-VCH

Table of Contents

FULL PAPER

CNTs@POP-salen core-shell nanostructure was constructed and successfully transferred to CNTs@POP-Co(salen). Owing to the shortened diffusion pathway, CNTs@POP-Co(salen) showed much higher activity than bulk polymer in propylene oxide hydration reaction (TOF: 3150 versus 1470 h^{-1}).

CNTs@POP-Co(salen) core-shell catalyst

Shortened diffusion pathway

Enhanced activity

TOF up to 5100 h^{-1}
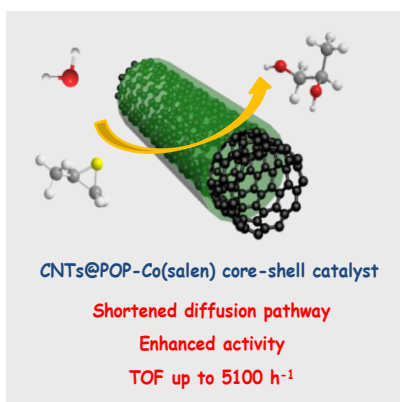
He Li, Mingmei Zhong, Chunzhi Li, Yiqi Ren, Jian Chen, Qihua Yang*

Page No. – Page No.

Synthesis of CNTs@POP-salen core-shell nanostructures for catalytic epoxides hydration